



TECHNICAL ARTICLE

Effect of Drag Finish Post-processing on Surface Integrity and Wear Behavior of Ti-6Al-4V Fabricated by Laser Powder Bed Fusion Additive Manufacturing

Emrah Güneşsu, Mustafa Safa Yılmaz , Emre Taşcıoğlu, Safian Sharif, and Yusuf Kaynak

Submitted: 17 January 2022 / Revised: 24 March 2022 / Accepted: 8 April 2022 / Published online: 25 July 2022

The Additive Manufacturing (AM) process provides opportunities to fabricate products with complex geometries including conformal cooling channels, etc. While having such an advantage, the low surface quality of the products is a disadvantage of laser powder bed fusion (LPBF). Because of that, a post-process is needed to improve the surface quality. Drag Finish (DF) is a surface enhancing operation based on removing small amounts of sawdust from the workpiece that is in contact with abrasive media. This study presents the effect of the drag finish post-processing parameters on wear and surface features of additively manufactured Ti-6Al-4V samples. Processing parameters considered are abrasive media, processing duration, and speed. This study reveals that the surface roughness of as-built specimens can be reduced up to 94% by implementing appropriate process parameters during post-processing operations. Drag finish also results in work hardening on the surface of the specimen and hence increased hardness of the treated surface by 6%. This eventually helps to improve the wear resistance of additively fabricated specimens.

Keywords additive manufacturing, drag finishing, laser powder bed fusion, post process, Ti-6Al-4V

1. Introduction

Additive Manufacturing (AM) is a type of production to ease complex-shaped pieces production and makes fast prototype production, especially in space, aviation, and biomedical (Ref 1, 2). Ti-6Al-4V alloy is one of the common materials used in these aforementioned industries. Moreover, it is a well-acknowledged fact that this material is difficult-to-machine material. Considering all these points, fabricating components made of Ti-6Al-4V alloy utilizing AM method is a reasonable and thus preferred approach. On the other hand, components manufactured through the AM process, including laser powder bed fusion, do not meet the surface requirements of the aforementioned industries. For such reason, post-processes operations such as turning (Ref 3), milling (Ref 4), tribofinish-

ing (Ref 5) (drag finishing, vibratory surface finish etc.), chemical treatment (Ref 6) and blasting (Ref 7) are widely used to enhance surface aspects of AM components

As a mass finishing process, drag finishing operations have been used in industry and academia for a long time for various purposes such as enhancing edge radius of cutting tools (Ref 8, 9), deburring operations of conventionally machined metal parts (Ref 10), surface polishing for conventionally fabricated parts, etc. (Ref 11). Few researchers also utilized it as post-processing operations to enhance the surface quality of additively manufactured stainless steel (Ref 12), maraging steel (Ref 13) and Inconel 718 (Ref 14). These studies reported that the drag finishing process improves surface aspects and topography of additively manufactured metal parts. These works also underlined that drag finishing process is much more efficient to improve surface properties than other tested post-processing operations including vibratory surface treatment. However, all these studies kept abrasive media constant and did not report the role of abrasive media on surface and subsurface aspects of additively manufactured parts. Abrasive media plays a major role in the effectiveness of the drag finishing process, as noted in previous studies that utilized the drag finishing process to improve surface aspects of conventionally manufactured metal components. Moreover, to the authors' best knowledge, no study investigates the influence of drag finishing on surface aspects of additively fabricated Ti-6Al-4V alloy.

Considering these points, the gap is evident. Furthermore, surface aspects are not limited to roughness and topography, and researchers also put efforts to modify and enhance the wear resistance of additively fabricated Ti-6Al-4V alloy (Ref 15) considering biomedical applications of this material (Ref 16). As drag finish is mass finishing operation and post-processing, its effect on wear resistance should also be investigated and reported. This present work aims to fill these gaps by presenting systematic experimental results focusing on the role of drag

Emrah Güneşsu, Department of Mechanical Engineering, Marmara University, 34854 Maltepe, Istanbul, Turkey; **Mustafa Safa Yılmaz**, Aluminium Test Training and Research Center (ALUTEAM), Fatih Sultan Mehmet Vakif University, Halic Campus, 34445 Istanbul, Turkey; **Emre Taşcıoğlu**, Research and Development Center, Torun Bakır Alaşımaları Metal San.ve Tic. A.Ş., İhsan Dede Cad. No:116, 41480 Gebze, Kocaeli Istanbul, Turkey; **Safian Sharif**, School of Mechanical Engineering, Universiti Teknologi Malaysia, 81310 Johor Bahru, Johor, Malaysia; and **Yusuf Kaynak**, Department of Mechanical Engineering, Marmara University, 34854 Maltepe, Istanbul, Turkey; and School of Mechanical Engineering, Universiti Teknologi Malaysia, 81310 Johor Bahru, Johor, Malaysia. Contact e-mail: m.safayilmaz@gmail.com.

finish process parameters and various abrasive media on surface properties of Ti-6Al-4V alloy produced by laser powder bed fusion additive manufacturing. Measured outputs are surface roughness, topography, microhardness and resulting wear resistance.

2. Materials and Methods

The specimens were composed of Ti-6Al-4V alloy powder and produced by Laser Powder Bed Fusion using EOS M 290 under Ar atmosphere. Specimens with equilateral triangle geometry with edge length 6 mm and height of 40 mm are fabricated. The particle size of powder used in this experiment was found to be in the range of 14-45 μm in diameter. Table 1 shows laser powder bed fusion (LPBF) process parameters for fabricating specimens. These laser parameters are recommended by EOS and commonly used for Ti-6Al-4V.

The drag finish post-processing technique is used to enhance the surface characteristics of LPBF processed specimens. Three different processing times (duration), two different rotational speeds and two different abrasive media were used for the DF process, as shown in Table 2. These drag finish process parameters and abrasive media are recommended by surface finishing machine manufacturer company considering Ti-6Al-4V work material and its properties. Future-Tech FM310, Keyence Digital Optical Microscope and Philips XI 30 Sfeq were used to measure microhardness, surface roughness, and wear marks, respectively. The microhardness of each sample was determined by an average of 4 measurements with a test load of 50 g using the Future-Tech FM310e model instrument with 15 s dwelling time.

The sliding wear tests were conducted using a reciprocating tribometer per the ASTM G133 standard. The tests were carried out for 40 min under a contact load of 10 N and a stroke length of 6 mm at room temperature in an air atmosphere without any cooling or lubricant. An Al_2O_3 abrasive ball was used for the reciprocating wear test. Since the hardness of the ball (1310 ± 10 HV) is much higher than that of the specimens, no wear of the carbide ball was observed during the test, and therefore it did not affect the wear behavior of the material.

3. Results and Discussion

3.1 Surface Roughness

The surface features of the components subjected to dynamic loads or contact forces are important, especially for the aviation, space, and biomedical industry qualifications (Ref

Table 1 LPBF process parameters for fabricating Ti-6Al-4Vspecimens

Laser power, W	195
Scan speed, mm/s	1250
Layer thickness, μm	30
Scan distance, μm	100
Building orientation, $^\circ$	60
Production strategy	Zigzag

14). Figure 1 shows the surface topographies of as-built specimens for both building and scanning directions. Partially melted powders attached to the surface layer of as-built specimens leads to undesired surface topographies on building direction. This is a commonly observed surface of specimens fabricated by the LPBF process. Much consistent surface is obtained on scanning direction that is also well acknowledged.

Figure 2 shows a 3-D examination of the Ti-6Al-4Vspecimen. As can be seen from the figure, the surface roughness value varies in a certain region. The average surface roughness value in building direction is $5 \pm 0.1 \mu\text{m}$. The overlapping layers and the dust adhering to the surface create a stair-step effect. Therefore, irregular and distorted profiles were formed (Ref 17).

The porous structure on the sample surface negatively affects fatigue under dynamic loads (Ref 18). The DF process decreases surface roughness depending on the operational parameters' adjustments.

In addition to experimentally measured surface roughness, theoretical calculation of surface roughness is also performed and presented in Fig. 3 by using the following equations proposed by Hashimoto (Ref 21).

$$R(t) = (I_r - D_r)e^{-t/T} + D_r \quad (\text{Eq 1})$$

The time constant T can be measured by the process time t when the surface roughness becomes the value $R(T)$ given by Eq 2.

$$R(T) = (I_r - D_r)e^{-1} + D_r \quad (\text{Eq 2})$$

The roughness of finished components can be predicted by using Eq 1 (time constant— T , roughness limitation (D_r , μm)), the best roughness value obtained during the processing period. Initial roughness (I_r , μm), initial roughness value measured from the as-built surface.

To estimate the surface roughness in this model, the system parameters such as the time constant T , the roughness limitation D_r can be measured from the experimental results shown in Fig. 3. System parameters measurements are presented in Table 3.

Considering experimental data shown in Fig. 3, it is obvious that post-processing time has notable effect on controlling surface roughness of additively fabricated components. Increasing post-processing time results in reduced surface roughness and thus improve surface quality for all tested abrasive media. The best surface quality was obtained after Al_2O_3 + plastic media/120 rpm/60 min DF treatment. This value is $0.30 \mu\text{m}$ and is approximately 94.1% less than as-built parts. With the increase of the operation time and fast rotational speed, large-sized plastic medias tend to decrease the surface roughness of the workpieces. The size of the abrasive media (plastic or Al_2O_3) and the shape of the abrasive media (conical, powder or nutshell) in the DF effect the impact energy on the sample and the higher energy decreasing the surface roughness (Ref 11, 19).

Different media used in abrasive environments and rotational speed also affect the surface roughness (Fig. 3a). With the increase of the cycle (Al_2O_3 media), the surface roughness value decreases at a rate of approximately 63.7%. In the 60 rpm cycle, Al_2O_3 + plastic media decreased the roughness value 74.5% compared to the Al_2O_3 media. However, at 120 rpm this value has appeared as 86%.

Table 2 DF process variables used in this study

	Al_2O_3 media, 100-175 μm	Plastic media, conical geometry $\varnothing 10 \times 10$ mm
Rotational speed, rotor, rpm	45	45
Rotational speed, workpiece, rpm	60, 120	60, 120
Processing time, min	15, 30, 60	15, 30, 60
Processing depth, cm	30	30

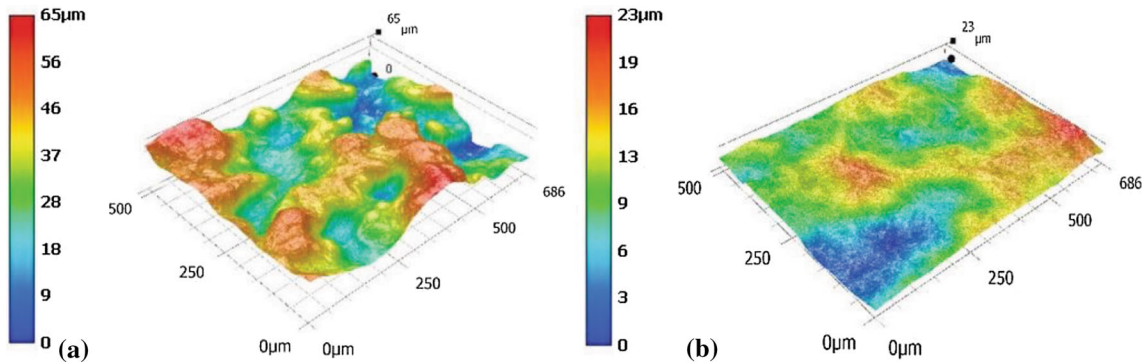


Fig. 1 Topography images of the building direction (a) and scanning direction (b) surfaces of Ti-6Al-4V samples

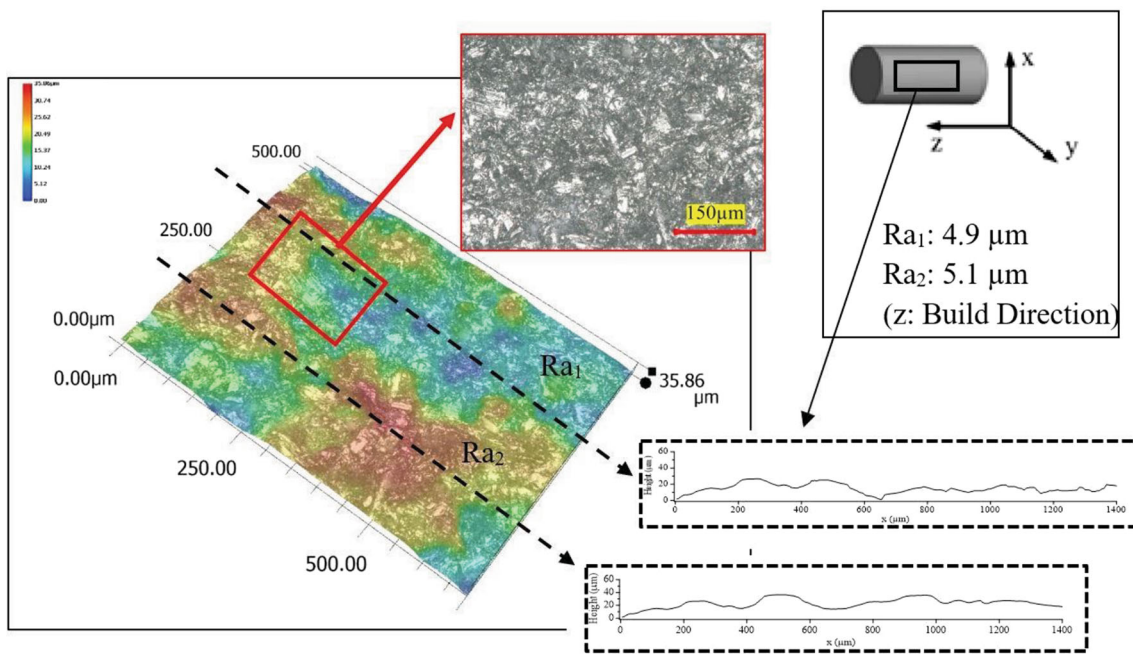


Fig. 2 Roughness measurement of as-built Ti-6Al-4V

In Fig. 3(b) and (c), the surface profile lines are compared using the Al_2O_3 and $Al_2O_3 +$ Plastic medias with different wear durations and cycles. With the cycle and process duration increase, the surface surges decreased and tended to be a straight line.

Calculated surface roughness values show reasonable agreement with the experimentally measured roughness values. The difference is varied between 4 and 24% that is found acceptable. But it should be noted that calculated surface roughness shows remarkable variation considering the first

15 min that is because of the poor surface quality of as-built samples resulting from partially melted powders stick to surface (Ref 20). However, as duration of post-processing time is increased to 30 and 60 min, the calculation offers much better agreement with experimentally measured data. For instance, considering 30 min post-processing duration, the difference between experimental data and calculated data is approximately 5%.

Surface images after the DF process of samples are shown in Fig. 4. Outer layer of samples include partially melted powders

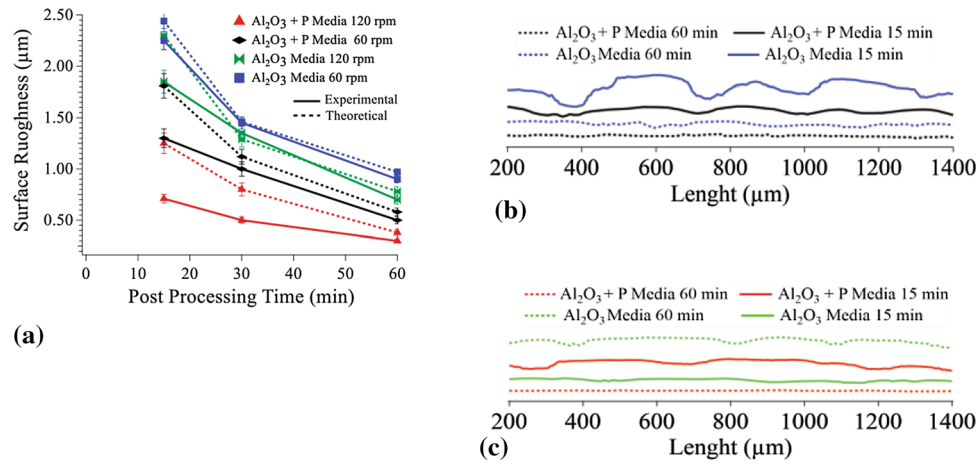


Fig. 3 (a) Surface roughness values after DF in different conditions, (b) Surface profile lines of samples surface treated using 60 rotational speed, (c) Surface profile lines of samples surface treated using 120 rotational speeds

Table 3 Constant values to be used in the surface roughness estimation model

Parameters	Al ₂ O ₃ , 60 rpm	Al ₂ O ₃ , 120 rpm	Al ₂ O ₃ + P, 60 rpm	Al ₂ O ₃ + P, 120 rpm
Time constant, <i>T</i> , min	15	15	15	15
Roughness limitation, <i>Dr Ra</i> , µm	0.9	0.7	0.5	0.3

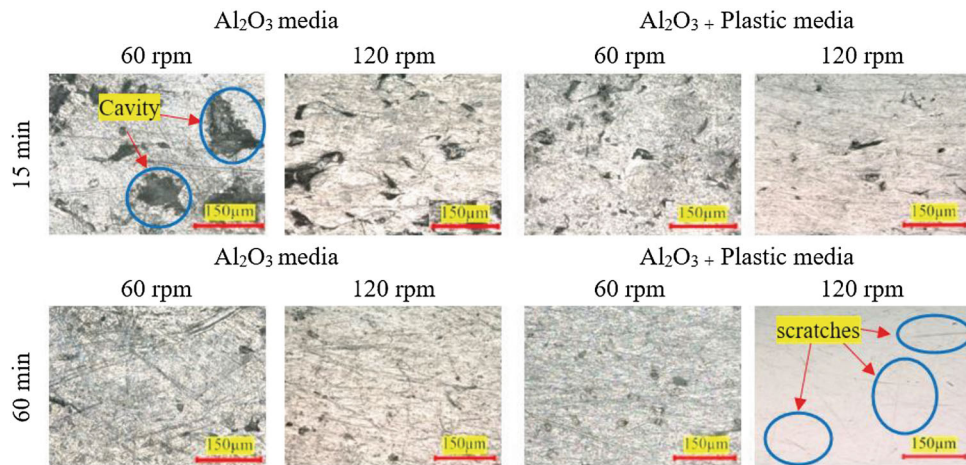


Fig. 4 Optical microscope images (2D) of DF processed workpieces

and cavities due to incomplete fusion (Ref 22). As can be seen, the DF parameters and abrasive media have had a serious impact on the surface quality. It has been observed that the use of plastic media has a positive effect on surface topography. While Al₂O₃ removes the surface layer effectively (Ref 5), large-sized plastic abrasive helps finishing the surface topography make the surface much smooth. This eventually helps to enhance surface quality by reducing surface roughness of samples. However, it is apparent that 15 min processing time by either using Al₂O₃ alone or Al₂O₃ and plastic media is not capable of removing the outer layer of samples. For this reason, surface topography does not seem to be perfect as yet. Increasing processing time substantially helps to improve the topography of samples as shown in Fig. 4. But at this point, the

role of plastic media is very critical. Utilizing plastic media along with Al₂O₃ at 120 rpm offers the best surface quality among all tested conditions. In this test, outer surface layer of samples is completely removed by Al₂O₃ as 60 min processing time is given and high rpm is implemented that generated larger kinetic energy (Ref 5, 19). Plastic media polished the generated new surface. But the remaining issue is scratches on the surface. Although it is not tested in this study, further processing by using only plastic media should be effective to remove these scratches from the surface.

3-D surface images of samples treated at 120 rpm and after 60 min operation time are shown in Fig. 5. Another interesting result is the scanning direction of the surfaces are not enhanced enough. The reason is dipping the workpieces to the DF

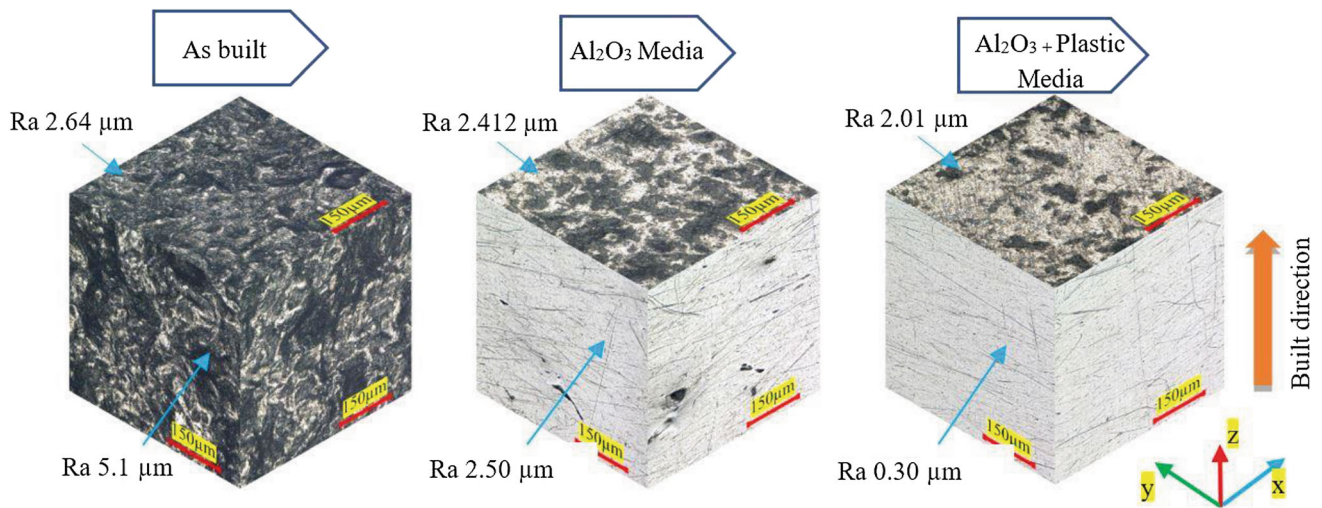


Fig. 5 Surface images formed after the DF process were applied for 60 min at 120 rpm

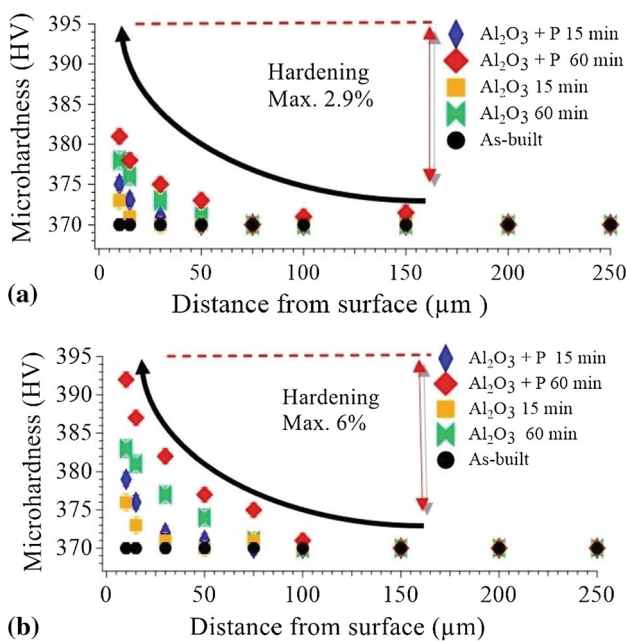


Fig. 6 Microhardness values; (a) at 60 rpm rotational speed, (b) at 120 rpm rotational speed

receptacle vertically. This situation is about the effects of the abrasive medias on the side surfaces effectively, but it cannot give the intended friction results in the bottom surface.

3.2 Microhardness

The surface and subsurface microhardness of as-built and treated samples at 60 and 120 rpm rotational speed are shown in Fig. 6. The hardness of as-built samples is approximately 370 HV. Results indicates that post-processing operations depending on processing time, rotational speed and media influences the surface and subsurface hardness of samples. While at lower rotational speed, process effected layer is approximately 50 μm beneath from the surface, it is approximately 100 μm when 120 rpm rotational speed is used. This is notable finding. Increase in percentage of hardness with

rotational speed also support this finding. For instance, maximum increase in hardness with using 60 rpm rotational speed is approximately 2.9%, it is almost 6% when 120 rpm rotational speed is used.

In addition to the rotational speed, abrasive media and processing time are also playing role on forming surface and subsurface hardness. It is an obvious that increasing processing time leads to generating harder surface and subsurface. For instance, maximum hardness measured at surface layer is approximately 378 HV when sample is treated Al_2O_3 + plastic with 15 min processing time, it is 392 HV when processing time increased to 60 min as shown in Fig. 6(b). Considering the role of abrasive on hardness variation, adding plastic media has some limited effect on increasing hardness. For instance, maximum hardness measured at surface layer is approximately 392 HV when sample is treated using Al_2O_3 + plastic with 60 min processing time, it is 383 HV when it is treated using only Al_2O_3 abrasive as shown in Fig. 6(b). Adding plastic media to abrasive polished the surface and likely increased residual stresses occurring on the surface (Ref 23). The same has been observed with the increase in the duration of the process (Ref 24).

As it is known, increase in hardness is the results of the formation of refined grains, and dislocation density increased due to plastic deformation (Ref 13). Our results show that major changes in hardness takes place at the surface region or just beneath the surface with longer processing time. Within such a long processing time and high rotational speed, much higher plastic deformation occurs and hence hardness becomes much higher than as-built sample.

4. Wear Behavior

4.1 Friction Coefficient

The wear process occurs in four zones, as described in Fig. 7. The first contact between the specimen and the abrasive ball is the running-in period (Ref 24), which occurs before wear reaches a stable state. This process is usually accompanied by a change in the coefficient of friction and wear rate (Ref 25). Since there is point contact between the specimen and the

Al₂O₃ abrasive ball, high pressure occurs and eventually causes rapid wear. It comes into direct contact with the oxide layer, and a rapid increase in the friction coefficient occurs (I. 0-20 s). It is thought that there is a decrease in the friction coefficient, and the oxide layer between the abrasive ball and the specimen prevents this reduction (II. between 20 and 60 s). As the contact area becomes larger, new contact surfaces are formed between the abraded material and the abrasive material during the wear process. Due to repetitive stress and load cycles, almost all the oxide layer is disintegrated and therefore, there is a significant increase in the friction coefficient. As a result of the disappearance of almost all the oxide layer, the Al₂O₃ ball and the sample are in full contact, and the increase in the friction coefficient continues (III. 60-150 s). Due to the surface contact area increase, the pressure between the sample and the Al₂O₃ wear ball decreases with time, and the friction coefficient becomes stable after about 100-150 s till the analysis end (Region IV). This stable character is also clearly shown in the wear test graphs of the study (Fig. 8).

The friction coefficient value of Ti-6Al-4V specimens obtained after the wear operation showed that it increased with the first contact at the start of the wear test and took a more stable form in the following test moments. The oscillations in the wear coefficient graphics can be explained as the activation of the wear mechanism of the Three-Body Effect caused by the oxide layer that occurred on the surface in the first place (Ref 26).

All the Coefficient of Friction (COF) graphs obtained are similar and can be seen in Fig. 8(a)-(b). The as-built specimens'

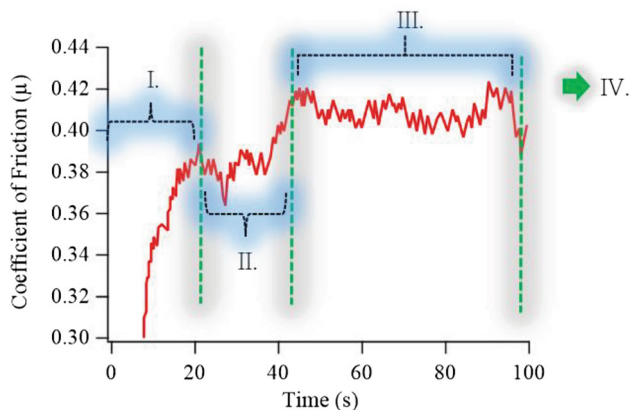


Fig. 7 Display of wear stages on the as-built workpiece

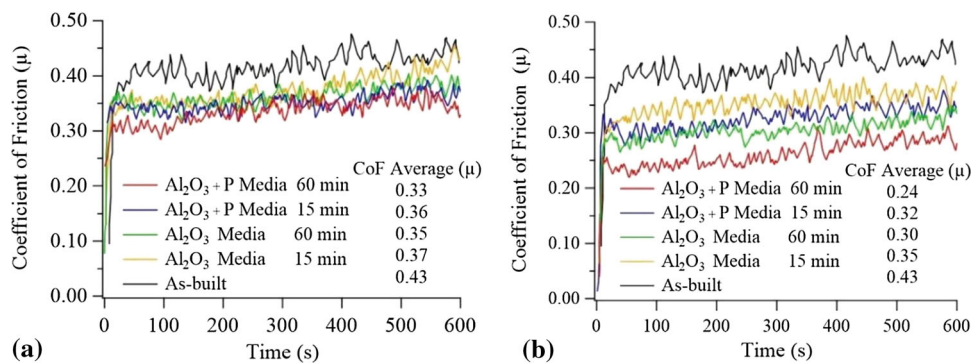


Fig. 8 The COF graph obtained because of the wear process (a) 60 rpm rotational speed, (b) 120 rpm rotational speed

COF graph showed more oscillations due to the surface quality that directly affects the contact between the wear ball and the worn (workpiece). If the contact established during the wear process is compatible, the flow of the formed wear residues on the worn surface will also be difficult (Ref 27). Due to the difficulty of flow on the contact surface during wear, abrasion residues sticking to the surface occur. These wear residues adhere to the wear surface and form a protective layer. This protective layer creates a harmonious contact and abrasion resistance between the abrasive and the wearer (Ref 28).

As a result, the strong effect of the contacts established between the geometries in contact on both the wear mechanism and the friction coefficient can be seen in Figure 8. The average friction coefficient values shown in Fig. 8 support this situation. The lowest COF value belongs to the Al₂O₃ + P medias/120 rpm/60 min DF process. Compared to the as-built specimen, the COF value decreased by 44.18%. The highest COF value belongs to the DF process that Al₂O₃ media/60 rpm/15 min parameters. Compared to the as-built specimen, the COF value decreased by 13.95% and at the same time, there was a 35.13% change between the conditions of Al₂O₃ + P medias/120 rpm/60 min. The irregular oscillations in the graphs can be explained in terms of third-body particles trapped between the abraded and abrasive sample during the wearing process (Ref 29). The friction coefficient value usually depends on the oxide layer on the surface, microstructure of the materials, microhardness and surface roughness, and it can develop depending on wear performance (Ref 30).

4.2 Wear Rate

Wear rates are calculated using Eq 3 and 4. The wear rates obtained from the calculations are shown in Fig. 9. Wear volume is calculated using Eq 3 as defined below (Ref 26).

$$V = L \left[r^2 \sin^{-1} \left(\frac{w}{2r} \right) - \frac{w}{2} \left(r^2 - \frac{w^2}{4} \right)^{\frac{1}{2}} \right] + \frac{\pi}{3} \left[2r^3 - 2r^2 \left(r^2 - \frac{w^2}{4} \right)^{\frac{1}{2}} - \frac{w^2}{4} \left(r^2 - \frac{w^2}{4} \right)^{1/2} \right] \quad (\text{Eq 3})$$

where V is the wear volume (mm³), r is the wear ball diameter, L is the stroke length, w is wear track width. The wear rate, k (mm³/Nm), is given by:

$$k = \frac{V}{Nxl} \quad (\text{Eq 4})$$

N indicates the applied force in Newton, l is the total distance traveled during wear as meter. The demonstration of the measurement of the wear width after the wear tests is presented in Fig. 10.

The wear rate calculation results are shown in Fig. 9. The wear rate obtained from the abrasion test performed on the as-built sample was calculated as $3.3 \times 10^{-2} \text{ mm}^3/\text{Nm}$. Three parameters increase the wear resistance of the surface in the DF process; use of Al_2O_3 + Plastic media, increase in process time, increase in rpm value. After the long duration of operation and resultant with combined surface enhancement stones, the thinned structure occurred on the surface, and the subsurface caused the material to harden (Fig. 6b). The higher the hardness value, the shallower the depth of the material crushed in the friction and wear process and the less the wear volume (Ref 31). Hardness measures resistance to plastic deformation without fracture under a hard indenter (Ref 32). The high microhardness (Al_2O_3 + Plastic media/120 rpm/60 min process) value resulted in the alloy's resistance to wear (Ref 30). However, more plastic deformation occurred because of the abrasion test performed on the as-built sample and the sample treated with Al_2O_3 media/60 rpm/15 min process. According to Archard's linear (Ref 33) law, the wear volume loss is inversely proportional to the hardness values of the worn material. The microhardness values obtained because of the secondary processing processes applied in this study (Fig. 6) are fully compatible with the wear rates obtained (Fig. 9). As a result, using combined surface enhancement stones and a long duration DF process gave fewer wear rates.

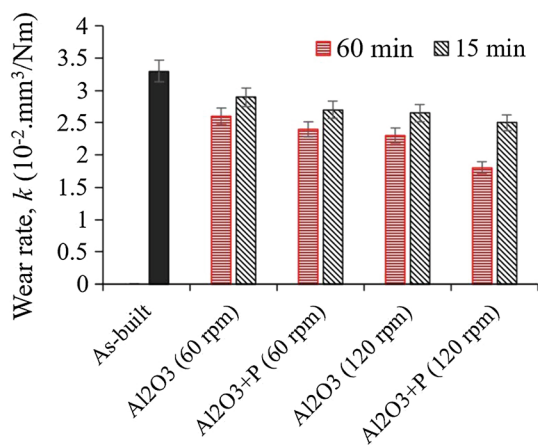


Fig. 9 The wear rates of the as-built and post-treated specimens

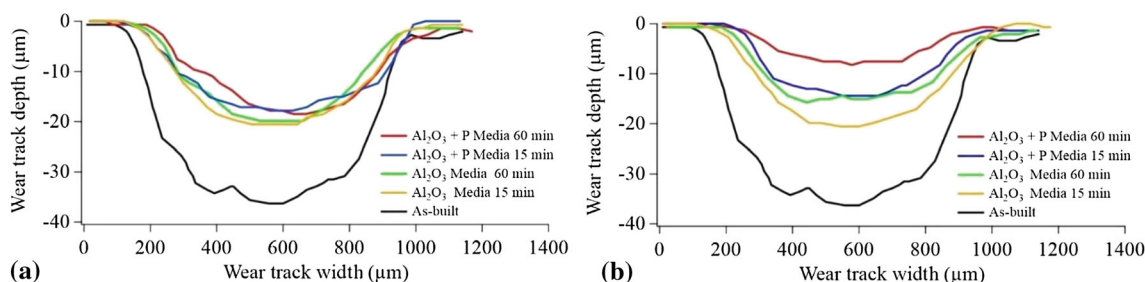


Fig. 10 Wear profile chart of workpieces subjected to DF process (a) 60 rpm rotational speed, (b) 120 rpm rotational speed

4.3 Wear Profile

The wear trace profiles are presented in Fig. 10. Wear trace & deepness showed differences with the DF process parameters. The as-built sample has the widest (0.967 mm) and deepest ($35.13 \mu\text{m}$) wear profile. The closest wear scar depth ($20.32 \mu\text{m}$) and width ($886.11 \mu\text{m}$) to the as-built sample belong to the sample applied Al_2O_3 media/60 rpm/15 min process. Depth of wear decreased by 42.15%, and wear width decreased by 8.3%. The lowest width ($669.45 \mu\text{m}$) and deepest ($7.29 \mu\text{m}$) belong to the sample applied Al_2O_3 + plastic media/120 rpm/60 min DF operation. Depth of wear decreased by 79.23% and wear width by 30.74%.

The increase in microhardness with the effect of post-processing plays a serious role in the wear rate case. Rough surfaces cause high friction force, and mechanical interaction increases with an increasing friction force. As a result, plastic deformation increases (Ref 34). As a result of the surface improvement processes, the different media used improved the surface quality depending on the rotation speed and processing time of the DF device. It also increased the microhardness value and wear resistance of surfaces.

SEM images of some wear marks are shown in Fig. 11(a)-(c). SEM images show differences in the tribological properties of the samples. Cracks and cavities cause delamination under and above the surface. The delamination wear mechanism occurs due to the shear deformation on the surface and the combination of cracks (Ref 35). Also, chip removal traces caused by wear are shown in Fig. 11(a). Crack propagation was observed in the transfer layer with the formation of delamination after wear. The delamination wear, which occurs because of the wear process applied to the as-built sample (Fig. 11a), is the porous structure on the surface and under the surface (Ref 36). In this case, it accelerates the formation of delamination, which causes a decrease in wear resistance.

Numerous fine scratches were observed on the inner surfaces of the groove formed in the wear track. The fact that the scratches are aligned along the sliding direction indicates abrasive wear (Ref 37). The relative extent of the grooves observed in the wear paths depends on the hardness of the abrasive body (Ref 26). When the SEM image of the sample, which was treated with Al_2O_3 + plastic medium/120 rpm/60 min, is examined, the wear groove is seen in Fig. 11(c). Due to these fine scratches aligned along the said slide direction, Abrasive wear is seen in Fig. 11(c). After the Al_2O_3 + plastic media/120 rpm/60 min DF process, no significant delamination was observed in the abrasion treated sample. However, in Al_2O_3 /60 rpm/15 min (the process with the worst surface), delamination occurred as shown in Fig. 11(b).

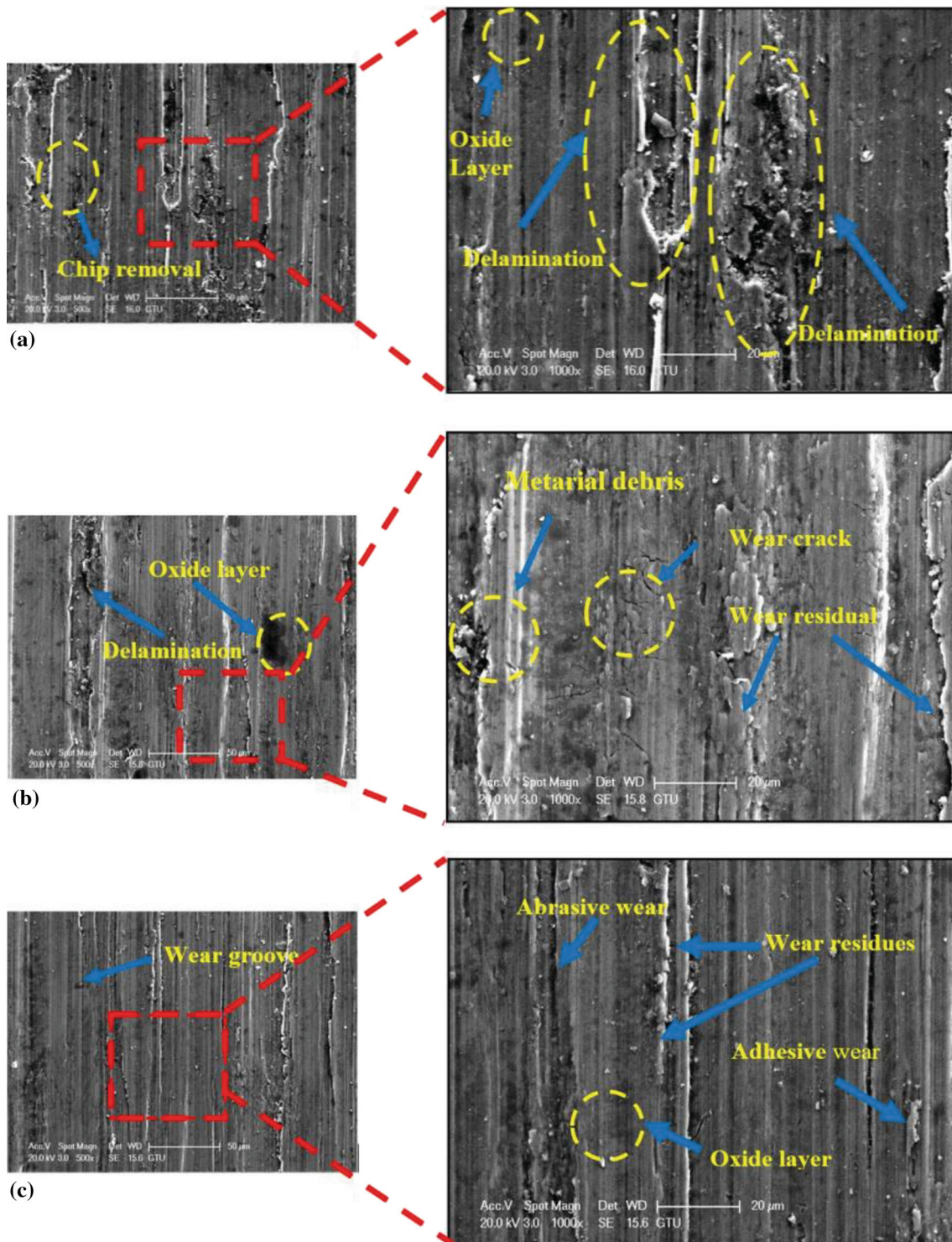


Fig. 11 Wear marks in SEM images (a) as-built (b) Al₂O₃ Media/60 rpm /15 min, (c) Al₂O₃ + P Media/120 rpm/60 min

The delamination of the as-built sample obtained due to the wear test is quite high compared to other results. Vertical cracks were formed in the transfer layer because of the wear load. Random clumps of material debris have formed on weathered surfaces because of the severe adhesive and abrasive wear (Ref 38). Concurrently during sliding, metal debris is crushed, mixed, and compacted into the worn surface, forming a tribolayer (Ref 39). A layer of tribo oxide is often found on the

corroded surface of Ti-6Al-4V. During the wear process, metal residues combine with oxygen, and the oxygen permeates the tribolayer. At the same time, delamination takes place resulting from the initiation and propagation of micro-scratches. In the wear process, micro-scratches are critically propagated, hence shear delamination occurs parallel with the worn surface and material debris from the worn surface (Ref 39).

5. Conclusions

In this study, the effect of drag finish post-processing parameters and abrasives media on the surface properties and resulting wear behavior of Ti-6Al-4V specimens fabricated by laser powder bed fusion was presented. This work demonstrates that the processing time and the abrasive media have substantial influence on measured outputs. Using Al_2O_3 + plastic media along with 120 rpm during 60 min processing time contributed to surface quality by reducing arithmetical average surface roughness from 5.1 to 0.30 μm . As a result of the DF operation performed under the same condition, the microhardness value increased by 6% (370 to 396 HV).

The calculated surface roughness by using the model borrowed from the literature for various abrasive media, process duration and rotational speed showed acceptable agreement with the experimentally measured average surface roughness value. It should be noted that while the model shows much better agreement with experiment when Al_2O_3 media is used, the difference between experimental result and calculated results becomes larger when Al_2O_3 + plastic media is used.

Wear resistance of specimens subjected to drag finish post-processing showed notable increase as compared to the wear resistance of as-built sample. Moreover, rotational speed and abrasive media play key role on further enhancing wear resistance of Ti-6Al-4V alloy fabricated by laser powder bed fusion. It should be also noted that post-processing operations along with process parameters and abrasive media substantially later wear mechanism of this Ti-6Al-4V alloy. For instance, while larger wear trace and formation of delamination observed on as-built specimen, abrasive and adhesive wears are observed on post-treated specimens. This work demonstrated that drag finish post-processing play remarkable role on enhancing wear resistance and controlling wear rate of additively manufactured Ti-6Al-4V alloy.

Acknowledgments

This work was also supported by the Research Project Program of Marmara University (BAPKO, Project FEN-C-YLP-250919-0271). Authors wish to thank to Marmara University and University Teknologi Malaysia for the collaboration in this research under the Grant Nos. 00P07 and 08G37.

References

1. D. Herzog et al., Additive Manufacturing of Metals, *Acta Mater.*, 2016, **117**, p 371–392. <https://doi.org/10.1016/j.actamat.2016.07.019>
2. B. Zhang, L. Dembinski and C. Coddet, The Study of the Laser Parameters and Environment Variables Effect on Mechanical Properties of High Compact Parts Elaborated by Selective Laser Melting 316L Powder, *Mater. Sci. Eng. A*, 2013, **584**, p 21–31. <https://doi.org/10.1016/j.msea.2013.06.055>
3. Y. Kaynak and O. Kitay, Porosity, Surface Quality, Microhardness and Microstructure of Selective Laser Melted 316L Stainless Steel Resulting From Finish Machining, *J. Manuf. Mater. Process.*, 2018, **2**(2), p 36. <https://doi.org/10.3390/jmmp2020036>
4. Y. Karabulut and Y. Kaynak, Drilling Process and Resulting Surface Properties of Inconel 718 Alloy Fabricated by Selective Laser Melting Additive Manufacturing, *Procedia CIRP*, 2020, **87**, p 355–359. <https://doi.org/10.1016/j.procir.2020.02.110>
5. F. Salvatore et al., Experimental and Numerical Study of Media Action During Tribofinishing in the Case of SLM Titanium Parts, *Procedia CIRP*, 2017, **58**, p 451–456. <https://doi.org/10.1016/j.jmbbm.2017.03.017>
6. B. Van Hooreweder et al., CoCr F75 Scaffolds Produced by Additive Manufacturing: Influence of Chemical Etching on Powder Removal and Mechanical Performance, *J. Mech. Behav. Biomed. Mater.*, 2017, **70**, p 60–67. <https://doi.org/10.1016/j.jmbbm.2017.03.017>
7. A. Triantaphyllou et al., Surface Texture Measurement for Additive Manufacturing, *Surf. Topogr. Metrol. Prop.*, 2015, **3**(2), p 024002. <https://doi.org/10.1088/2051-672X/3/2/024002>
8. O. Hronek et al., Influences of Holders Speed on the Cutting Edge During Drag Finishing, *Manuf. Technol.*, 2016, **16**(5), p 933–939. <https://doi.org/10.21062/ujep/x.2016/a1213/MT/16/5/933>
9. P.C. Priarone et al., Effects of Cutting Angle, Edge Preparation, and Nano-Structured Coating on Milling Performance of a Gamma Titanium Aluminum, *J. Mater. Process. Technol.*, 2012, **212**(12), p 2619–2628. <https://doi.org/10.1016/j.jmatprotec.2012.07.021>
10. E. Uhlmann and M. Kopp, Measurement and Modeling of Contact Forces during Robot-guided Drag Finishing, *Procedia CIRP*, 2021, **102**, p 518–523. <https://doi.org/10.1016/j.procir.2021.09.088>
11. I. Malkorra et al., The Influence of the Process Parameters of Drag Finishing on the Surface Topography of Aluminium Samples, *CIRP J. Manuf. Sci. Technol.*, 2020, **31**, p 200–209. <https://doi.org/10.1016/j.irpj.2020.05.010>
12. Y. Kaynak and O. Kitay, The Effect of Post-Processing Operations on Surface Characteristics of 316L Stainless Steel Produced by Selective Laser Melting, *Addit. Manuf.*, 2019, **26**, p 84–93. <https://doi.org/10.1016/j.addma.2018.12.021>
13. H. Khan et al., The Impact of Aging and Drag-Finishing on the Surface Integrity and Corrosion Behavior of the Selective Laser Melted Maraging Steel Samples, *Materialwiss. Werkstofftech.*, 2021, **52**(1), p 60–73. <https://doi.org/10.1002/mawe.202000139>
14. Y. Kaynak and E. Tascioglu, Post-Processing Effects on the Surface Characteristics of Inconel 718 Alloy Fabricated by Selective Laser Melting Additive Manufacturing, *Prog. Addit. Manuf.*, 2020, **5**(2), p 221–234. <https://doi.org/10.1007/s40964-019-00099-1>
15. A.S. Patil et al., Effect of TiB₂ Addition on the Microstructure and Wear Resistance of Ti-6Al-4V Alloy Fabricated Through Direct Metal Laser Sintering (DMLS), *J. Alloys Compd.*, 2019, **777**, p 165–173. <https://doi.org/10.1016/j.jallcom.2018.10.308>
16. J. Ju et al., Tribological Investigation of Additive Manufacturing Medical Ti₆Al₄V Alloys Against Al_2O_3 Ceramic Balls in Artificial Saliva, *J. Mech. Behav. Biomed. Mater.*, 2020, **104**, p 103602. <https://doi.org/10.1016/j.jmbbm.2019.103602>
17. G. Strano et al., Surface Roughness Analysis, Modelling and Prediction in Selective Laser Melting, *J. Mater. Process. Technol.*, 2013, **213**(4), p 589–597. <https://doi.org/10.1016/j.jmatprotec.2012.11.011>
18. M. Xia et al., Influence of Hatch Spacing on Heat and Mass Transfer, Thermodynamics and Laser Processability During Additive Manufacturing of Inconel 718 Alloy, *Int. J. Mach. Tools Manuf.*, 2016, **109**, p 147–157. <https://doi.org/10.1016/j.ijmactools.2016.07.010>
19. M. Barletta et al., A Comparative Evaluation of Fluidized Bed Assisted Drag Finishing and Centrifugal Disk Dry Finishing, *Eng. Sci. Technol. Int. J.*, 2014, **17**(2), p 63–72. <https://doi.org/10.1016/j.jestch.2014.03.007>
20. D. Ding et al., Wire-Feed Additive Manufacturing of Metal Components: Technologies, Developments and Future Interests, *Int. J. Adv. Manuf. Technol.*, 2015, **81**(1), p 465–481. <https://doi.org/10.1007/s00170-015-7077-3>
21. F. Hashimoto and D.B. DeBra, Modelling and Optimization of Vibratory Finishing Process, *CIRP Ann.*, 1996, **45**(1), p 303–306. [https://doi.org/10.1016/S0007-8506\(07\)63068-6](https://doi.org/10.1016/S0007-8506(07)63068-6)
22. B. Zhang, Y. Li and Q. Bai, Defect Formation Mechanisms in Selective Laser Melting: A Review, *Chin. J. Mech. Eng.*, 2017, **30**(3), p 515–527. <https://doi.org/10.1007/s10033-017-0184-3>
23. D.T. Ardi et al., Investigations of the Residual Stresses and Surface Integrity Generated by a Novel Mechanical Surface Strengthening, *Residual Stresses 2016*, 2017 <https://doi.org/10.21741/9781945291173-53>
24. A. Khorasani et al., The Effect of SLM Process Parameters on Density, Hardness, Tensile Strength and Surface Quality of Ti-6Al-4V, *Addit. Manuf.*, 2019, **25**, p 176–186. <https://doi.org/10.1016/j.addma.2018.09.002>

25. O. Zambrano et al., Running-in Period for the Abrasive Wear of Austenitic Steels, *Wear*, 2020, **452**, 203298. <https://doi.org/10.1016/j.wear.2020.203298>
26. F. Bartolomeu et al., Wear Behavior of Ti6Al4V Biomedical Alloys Processed by Selective Laser Melting Hot Pressing and Conventional Casting, *Trans. Nonferrous Metals Soc. China*, 2017, **27**(4), p 829–838. [https://doi.org/10.1016/S1003-6326\(17\)60060-8](https://doi.org/10.1016/S1003-6326(17)60060-8)
27. C. Mary et al., Pressure and Temperature Effects on Fretting Wear Damage of a Cu-Ni-In Plasma Coating Versus Ti17 Titanium Alloy Contact, *Wear*, 2011, **272**(1), p 18–37. <https://doi.org/10.1016/j.wear.2011.06.008>
28. R. Merhej and S. Fouvry, Contact Size Effect on Fretting Wear Behaviour: Application to an AISI 52100/AISI 52100 Interface, *Lubr. Sci.*, 2009, **21**(3), p 83–102. <https://doi.org/10.1002/lvs.74>
29. J. Silva et al., Corrosion and Tribocorrosion Behavior of Ti-TiB-TiN_x in-Situ Hybrid Composite Synthesized by Reactive Hot Pressing, *J. Mech. Behav. Biomed. Mater.*, 2017, **74**, p 195–203. <https://doi.org/10.1016/j.jmbbm.2017.05.041>
30. Z. Wang et al., Influence of Ultrasonic Surface Rolling on Microstructure and Wear Behavior of Selective Laser Melted Ti-6Al-4V Alloy, *Materials*, 2017, **10**(10), p 1203. <https://doi.org/10.3390/ma10101203>
31. S. Ehtemam-Haghighi et al., Evaluation of Mechanical and Wear Properties of Ti_xNb₇Fe Alloys Designed for Biomedical Applications, *Mater. Des.*, 2016, **111**, p 592–599. <https://doi.org/10.1016/j.matdes.2016.09.029>
32. H. Li, M. Ramezani and Z.W. Chen, Dry Sliding Wear Performance and Behaviour of Powder Bed Fusion Processed Ti-6Al-4V Alloy, *Wear*, 2019, **440**, p 203103. <https://doi.org/10.1016/j.wear.2019.203103>
33. I. Hutchings, *Tribology: Friction and Wear of Engineering Materials*, Butterworth-Heinemann, Oxford, 1992, p 78–84
34. M. Uçurum et al., Farklı kesme parametreleriyle işlenmiş 316LVM paslanmaz çelik malzemesinin talaşlı imalat-yüzey bütünlüğü-aşınma direnci arasındaki ilişkinin incelenmesi, *Pamukkale Üniversitesi Mühendislik Bilimleri Dergisi.*, 2021, **27**(4), p 449–545. <https://doi.org/10.5505/pajes.2020.93284>
35. N.P. Suh, The Delamination Theory of Wear, *Wear*, 1973, **25**(1), p 111–124. [https://doi.org/10.1016/0043-1648\(73\)90125-7](https://doi.org/10.1016/0043-1648(73)90125-7)
36. J. Yang et al., Role of Molten Pool Mode on Formability, Microstructure and Mechanical Properties of Selective Laser Melted Ti-6Al-4V Alloy, *Mater. Des.*, 2016, **110**, p 558–570. <https://doi.org/10.1016/j.matdes.2016.08.036>
37. P. Podra and S. Andersson, Simulating Sliding Wear With Finite Element Method, *Tribol. Int.*, 1999, **32**(2), p 71–81. [https://doi.org/10.1016/S0301-679X\(99\)00012-2](https://doi.org/10.1016/S0301-679X(99)00012-2)
38. P. Mercelis and J.P. Kruth, Residual Stresses in Selective Laser Sintering and Selective Laser Melting, *Rapid Prototype. J.*, 2006 <https://doi.org/10.1108/13552540610707013>
39. G.D. Revankar et al., Wear Resistance Enhancement of Titanium Alloy (Ti-6Al-4V) by Ball Burnishing Process, *J. Market. Res.*, 2017, **6**(1), p 13–32. <https://doi.org/10.1016/j.jmrt.2016.03.007>

Publisher's Note Springer Nature remains neutral with regard to jurisdictional claims in published maps and institutional affiliations.